Seamless Accurate Positioning in Deep Urban Area Based on Mode Switching Between DGNSS and Multipath Mitigation Positioning

Yongjun Lee, *Graduate Student Member, IEEE*, Yoola Hwang, Jae Young Ahn, Jiwon Seo, *Member, IEEE*, and Byungwoon Park, *Member, IEEE*

***Abstract*— Multipath and non-line-of-sight (NLOS) signals are the major causes of poor accuracy of a global navigation satellite system (GNSS) in urban areas. Despite the wide usage of the GNSS in populated urban areas, it is difficult to suggest a generalized method because multipath errors are user-specific and cannot be eliminated by the differential GNSS (DGNSS) or a real-time kinematic technique (RTK). This paper introduces a real-time multipath estimation and mitigation technique which considers compensation for the time offset between constellations. It also presents a mode-switching algorithm between the DGNSS and multipath mitigating mode and shows that this technique can be effectively utilized for automobiles in a deep urban environment without any help from sensors other than GNSS. The availability is improved from 64% to 100% and the error RMS is reduced from 11.1 m to 1.2 m on Teheran-ro, Seoul, Korea. Because this method does not require prior information or additional sensor implementation for high-positioning performance in deep urban areas, it is expected to gain wide usage in not only the automotive industry but also future intelligent transportation systems.**

***Index Terms*— Deep urban area positioning, differential GNSS, global navigation satellite system, multipath, non-line-of-sight error.**

I. Introduction

GLOBAL navigation satellite system (GNSS) is the underlying technology of intelligent transportation system (ITS) [1], which is widely used in various fields such as autonomous vehicles [2] and unmanned air systems (UASs) [3], [4]. By 2050, more than two-thirds of the world population is expected to reside in urban areas [5], leading to increase in GNSS-based services offered in urban environments [2]; therefore, the demand for improving the GNSS accuracy in urban canyons is gradually increasing. However, the positioning performance in urban canyons is inevitably much worse than that under the open sky because GNSS positioning is neither reliable nor accurate if satellite signals are blocked and/or reflected [6]. Accurate positioning in urban areas is a long-standing problem of the GNSS. When the reflected signals are received together with the direct signal, they interfere with the signals received directly from the satellites [7]; this phenomenon is generally called multipath. In addition to the typical phenomenon of multipath, non-line-of-sight (NLOS) cases, in which the direct signal is blocked and only the reflected signal is received [7], frequently occur in urban areas. In this study, both cases are called multipath for convenience.

Multipath is a site-dependent error similar to receiver noise, which cannot be eliminated by a differential technique such as RTK or DGNSS [8]. Unlike the common GNSS errors removable through differential methods, the effect of the site-specific error is sensitively dependent on the signal reception environment. Reflective surfaces also affect the signals, which can be scattered [9] or diffracted [10] rather than simply being reflected. Thus, it is highly challenging to mitigate or model the multipath, which makes it a dominant source of error in urban canyons. When GNSS signals are prone to reflection due to the presence of numerous vehicles and buildings, these effects may cause a positioning error of approximately 100 m in urban canyons [11]. The NLOS-type multipath makes receivers perceive the measurement that includes the reflected path as directly observable [7], which can cause errors of several hundred meters in a deep urban canyon.

Low satellite visibility and poor geometry are other problems in urban GNSS positioning. Satellites are prone to be shadowing in urban areas due to high-rise buildings, and poor satellite visibility and lower number of visible satellites reduce both the availability and accuracy of GNSS positioning [12], [13]. Moreover, only the satellites along the track of the street are visible because of signal blocking by the buildings on both sides of the street, which makes the error

Manuscript received 11 November 2021; revised 12 July 2022 and 30 December 2022; accepted 20 February 2023. Date of publication 4 April 2023; date of current version 31 May 2023. This work was supported in part by the Ministry of Science and ICT (MSIT), South Korea, under the Information Technology Research Center Support Program supervised by the Institute for Information & Communications Technology Planning & Evaluation under Grant IITP2020-2018-0-01423; and in part by the Unmanned Vehicles Core Technology Research and Development Program through the National Research Foundation of Korea (NRF) and Unmanned Vehicle Advanced Research Center (UVARC) funded by MSIT under Grant 2020M3C1C1A01086407. The Associate Editor for this article was Z. M. Kassas. *(Corresponding author: Byungwoon Park.)*

Yongjun Lee and Byungwoon Park are with the Department of Aerospace Engineering and Convergence Engineering for Intelligent Drone, Sejong University, Seoul 05006, Republic of Korea (e-mail: byungwoon@sejong.ac.kr).

Yoola Hwang is with the Satellite Navigation Research Section, Electronics Telecommunications Research Institute, Daejeon 34129, Republic of Korea (e-mail: ylhwang@etri.re.kr).

Jae Young Ahn is with the Unmanned Vehicle Research Section, Electronics Telecommunications Research Institute (ETRI), Daejeon 34129, Republic of Korea (e-mail: jyahn@etri.re.kr).

Jiwon Seo is with the School of Integrated Technology, Yonsei University, Incheon 21983, Republic of Korea (e-mail: jiwon.seo@yonsei.ac.kr).

Digital Object Identifier 10.1109/TITS.2023.3256040

ellipse excessively elongated in the cross-track direction of the road [14], [15]. The influence of the geometrical distribution of satellites around the users [16] is considered a primary factor in lowering the GNSS positioning integrity [17]. Owing to miniscule number of redundant satellites and poor satellite geometry, the multipath errors of some satellites cannot be hidden in the position error; instead, they are more apparent than under the open sky, making the calculated position unreliable.

Recently, various studies have attempted to mitigate the multipath effect by using additional equipment such as fish-eye lens, inertial navigation system (INS), visual camera, long-term evolution (LTE), and light detection and ranging (LiDAR). Even though a fish-eye lens could distinguish between the LOS and NLOS satellites [18], [19], [20], the GNSS receiver with an embedded fish-eye lens is difficult for universal utilization, and various weather conditions such as sun glare, rain and night present different challenges in clearly distinguish buildings. Kalman filter-based GNSS/INS integration has been one of the most traditional solution to mitigate multipath [21], [22], [23], [24]. Factor graph optimization recently showed better performance in urban scenario [25], [26], [27]. However, the INS-integrated technique often failed to compute accurate solutions to overcome the multipath in deep urban areas if the vehicle drove with frequent stops or without updating the GNSS solutions for a long duration [9], [28]. Environmental features obtained from LiDAR were used to quantify multipath on GNSS signals in urban environment [29], [30]. LTE-based techniques are particulary attractive because they don't require any infrastructure. If appropraitely utilized, they can result in a practical, economical, and accurate localization system [31]. However, the sensors integrated into the navigation systems employing GNSS were able to compute only the relative position; therefore, it is necessary to apply the absolute position [32], [33] provided by GNSS before time-updating. The accuracy of the integrated navigation system eventually depends on the GNSS; therefore, it is important to improve the absolute position accuracy of the GNSS in urban canyons.

Three-dimensional (3D) building information improves the accuracy of the GNSS absolute position in urban canyons; in addition, techniques such as shadow matching and ray tracing have been introduced. Shadow matching utilizes the 3D building information to check the visibility of each satellite based on the geometry formed by the user location, surrounding buildings, and GNSS signal direction [31], [33], [34]. The ray-tracing technique estimates and mitigates the pseudorange multipath errors by using all possible reflected rays from the satellite to the receiver based on the 3D building information [35]. Because ray tracing directly estimates the error of the NLOS signal, it has the advantage of mitigating the error without damaging the positioning availability.

The biggest challenge in shadow matching and ray tracing is their overwhelming computational load [10]. Because multipath errors vary depending on the signal reception position, both methods assign candidates near the initially calculated position and then exclude or compensate for the NLOS pseudorange observable for all the position candidates. Only the exact position among the candidates eventually enables the exclusion and compensation of the NLOS errors to accurately compute the position; this problem was called the chicken–egg problem by van Diggelen [10]. Thus, for integration with additional sensors, the position accuracy of the GNSS is vital for successful integration with information in urban areas.

There are many traditional techniques for mitigating multipath by using only GNSS measurements, namely, receiver-internal correlation, multi-constellation, measurement weighting, consistency checking, and averaging, as summarized in Table I. In urban environment, there may be several extra delayed replicas along with LOS signal, which causes an asymmetry correlation function and eventually leads to error in range calculation. The multipath mitigation technique using the double differentiated correlation function-based histogram approach showed improved accuracy in general multipath scenarios [36]. Multi-constellation is the simplest way to mitigate the multipath effect on the position results [37] and improve the availability, accuracy, and robustness in urban areas by increasing the number of available satellites [21]. The weighting technique based on the elevation angle or signal strength of each satellite is another widely used technique for mitigating the multipath effect [38]. However, the multi-constellation and/or weighting are/is effective in conveniently mitigating the influence of the multipath errors on the position rather than the multipath itself and are therefore ineffective when more than a few satellites are available.

Integrity control techniques, such as receiver autonomous integrity monitoring (RAIM) based on the measurement residuals, can also be used to exclude the satellite with the largest residual error caused by the multipath error [39]. The conventional RAIM algorithm assumes many redundancies and no more than one failure; however, it is highly difficult to apply to urban signal reception environments [16]. The monitoring code minus carrier (CMC) can be used as another metric to measure multipath variations [40]. Because this technique assumes that the multipath errors accumulated over a long period have a Gaussian distribution, it is necessary to solve the carrier ambiguity by averaging the CMC to calculate and correct the error. However, this assumption is acceptable only when long-term data have been accumulated, and the averaged value of multipath and NLOS errors in urban areas cannot be zero in urban areas.

Despite the imperfectness of the assumption in the existing CMC method, our previous study focused on the availability of CMC to observe the multipath variation [41]. Once the initial multipath is computed correctly, the CMC variation enables the update of the multipath error, which directly mitigates the error regardless of LOS or NLOS. However, the technique proposed in the previous studies has two main challenges. One is the algorithm must start at known coordinates for the estimation filter initialization, and the other is the multipath estimation uncertainty can accumulate gradually when the filter is processed for a long time.

TABLE I
MULTIPATH MITIGATION TECHNIQUES USING ONLY GNSS MEASUREMENT

Classification	Technique	Accuracy	Availability
Sparse Estimating [36] [37] [38]	- Receiver-internal correlation - Measurement Weighting - Multi-Constellation	54% improved	No loss of availability
Multipath Detection & Exclusion [32] [39]	- Consistency Checking - NLOS Signal Detection and Exclusion	29~31% improved	Loss of availability
Stochastic Weighting [40] [41]	- Averaging CMC - CMC Variation	10~60% improved	No loss of availability

In this study, we propose a method for mode switching between DGNSS and CMC-based multipath mitigation to solve the inherent and chronic problem of the previous algorithms. The DGNSS residual-based validation test enables the switching algorithm to check the current signal environment and then determine a suitable positioning mode. Once the algorithm determines that the current GNSS observables are reliable, the DGNSS is activated for the current positioning mode. However, when the DGNSS position does not pass the validation test, the mode should be changed to CMC-based multipath mitigation mode until the DGNSS is again determined to be valid. The proposed method in this study uses only GNSS measurements without any information including initial coordinates or sensors other than GNSS, and this method corresponds to the stochastic weighting in Table I that improves positioning accuracy and does not reduce positioning availability.

The main contributions of this study are:

1) Determining the signal receiving environment by the DGNSS residual-based validation test without requiring any additional sensor.
2) Adaptive switching of the positioning mode between the CMC-based multipath mitigation and DGNSS according to the signal receiving environment in dense urban area.
3) Providing a reliable and optimal solution by flexible integration of CMC-based multipath migration technique and DGNSS.

The remainder of this paper is organized as follows. In Section II, a seamless multipath estimation methodology is described, considering deep urban applications. Section III presents the multipath mitigation and positioning method with its mode-switching technique. A field test was conducted in Teheran-ro, Seoul, Korea, and the results are examined in Section IV. The discussion and conclusions are presented in Section V.

II. MULTIPATH ESTIMATION METHODOLOGY FOR URBAN ENVIRONMENTS

A. Consecutive Multipath Estimation Using GNSS CMC Variation

The GNSS correlation peak can be distorted when a reflected signal is received with the direct signal, causing multipath interference. The maximum error in pseudorange measurements is equal to half of a ranging code chip, approximately 150 m, and the carrier phase error can reach a quarter of a wavelength, which is 4.76 cm for the GPS L1 frequency [42]. When an NLOS signal is received solely without a direct signal, the receiver mistakes the received signal as a direct signal. In this case, the reflected signal path length is induced into the range error; thus, there is no limit on the maximum error, which can be up to several kilometers. Except for the cycle slip case due to the transition between LOS and NLOS, the carrier-phase multipath error remains limited to half the cycle of the wavelength (modulo one carrier cycle) [7]. On the receiver side, the error-inducing mechanism, range of the LOS multipath interference, and NLOS reflected range error are very different from each other; however, the error terms are included in the measurements in the same format and cause positioning errors in the same manner. In this paper, we collectively call both errors induced by these two reflected signals, i.e., LOS and NLOS signals, as multipath.

The multipath error (M^i) for the i-th satellite is included in the GNSS code observable (ρ_f^i) for frequency f, as described in (1). Similarly, the carrier phase multipath error (m_f^i) is included in (2), which is much smaller than M^i for both LOS and NLOS cases.

The pseudorange code measurement and carrier phase measurement of the i-th satellite at time t can be modeled as (1) and (2).

$$\rho_f^i(t) = d^i(t) + \left(B(t) - b^i(t)\right) + I_f^i(t) + T^i(t) + M_f^i + \epsilon_f^i \tag{1}$$

$$\phi_f^i(t) = d^i(t) + \left(B(t) - b^i(t)\right) - I_f^i(t) + T^i(t) + m_f^i + N_f^i\lambda_f + \varepsilon_f^i \tag{2}$$

where d is the distance between the receiver and satellite, and B and b are the receiver and satellite clock errors, respectively. I and T denote the ionospheric and tropospheric errors, respectively. The measurement noise values of the pseudorange and carrier phases are represented by ϵ and ε. N and λ in the carrier phase modeling equation are the integer ambiguity and wavelength, respectively, for the frequency f.M and m represent the multipath errors included in the pseudorange and carrier phase measurements, respectively.

Because the ionospheric delay included in GNSS measurements is proportional to the square of frequency ratio, linearly combining the code and phase measurements of the L1 and L2 frequencies in (1) and (2), removes the ionospheric errors in both the code and carrier measurements, which results in the ionosphere-free linear combination equations (3) and (4).

$$\rho_{if}^i(t) = \frac{\rho_{L1}^i(t)\cdot\gamma - \rho_{L2}^i(t)}{\gamma - 1} = d^i(t) + \left(B(t) - b^i(t)\right) + T^i(t) + M_{if}^i(t) + \epsilon_{if}^i(t) \tag{3}$$

$$\phi_{if}^i(t) = \frac{\phi_{L1}^i(t)\cdot\gamma - \phi_{L2}^i(t)}{\gamma - 1} = d^i(t) + \left(B(t) - b^i(t)\right) + T^i(t) + m_{if}^i(t) + \varepsilon^i(t) + \frac{\lambda_{L1}N_{L1}^i(t)\cdot\gamma - \lambda_{L2}N_{L2}^i(t)}{\gamma - 1} \tag{4}$$

where γ is the square of the L1/L2 frequency ratio, that is, f_{L1}^2/f_{L2}^2, and the subscript if represents the ionosphere-free combined measurement.

If a rover's position at the initial time t_0 has been computed exactly, the initial value of the multipath error that corrupts the pseudorange code observable can be calculated as shown in (5). In the initial multipath error estimation, the distance ($\hat{d}^i$) from the rover's initial position to each satellite and the tropospheric error ($\hat{T}^i$) computed by the Saastamoinen model [43] are used. The satellite clock bias $\hat{b}^i_{if}$ is corrected for the ionosphere-free combination by using the received navigation message. The rover's clock bias can be mitigated using $\hat{B}$ from the navigation solution as shown in (5), which may cause a bias in the multipath initial estimate because $\hat{B}$ cannot be accurate. However, the bias is common to all satellites; thus, it does not harm the rover's position accuracy.

$$\hat{M}^i_{if}(t_0) \approx \rho^i_{if}(t_0) - \hat{d}^i(t_0) - \left(\hat{B}(t_0) - \hat{b}^i_{if}(t_0)\right) - \hat{T}^i(t_0) \tag{5}$$

Once the initial value of the pseudorange multipath has been estimated, its values can be updated using the CMC variation. The CMC process enables the removal of the geometry terms, that is, distance, clock offsets, and tropospheric error, which results in the modeling equation (6) comprising the code and carrier multipath. It should be noted that the code multipath error is incomparably much larger than that of the carrier phase. Thus, a simpler equation is obtained, as shown in (7), which is mainly composed of the code multipath and ambiguity of the carrier phase.

$$CMC^i_{if}(t) = \rho^i_{if}(t) - \phi^i_{if}(t) = M^i_{if}(t) - m^i_{if}(t) - N^i_{if}(t)\lambda_{if} + \epsilon^i_{if}(t) - \varepsilon^i_{if}(t) \tag{6}$$

$$CMC^i_{if}(t) \approx M^i_{if}(t) - N^i_{if}(t)\lambda_{if} + \epsilon^i_{if}(t) - \varepsilon^i_{if}(t) \tag{7}$$

If the receiver has not lost its continuous carrier tracking while maneuvering in the urban canyons, the cycle of the carrier would not slip, and the ambiguity term remains constant. Because the time difference (TD) of the carrier ambiguity, $\Delta N^i_{if}(t)\lambda_{if}$, is zero under the condition that no cycle slip occurs in the i-th satellite carrier observation, the variation in the code multipath, ΔM_{if}, is almost the same as the CMC variation, as shown in (8).

$$\Delta CMC^i_{if}(t) \approx \Delta M_{if}(t) \tag{8}$$

We can calculate the code multipath error for the i-th satellite at time t by accumulating the CMC variation from the initial value obtained from (5). Because we suggest using the ionosphere-free combination measurements, unlike other studies, the suggested multipath calculation of (9) is free from ionospheric divergence even if it is accumulated for a long time.

$$M^i_{if}(t_k) \approx M^i_{if}(t_0) + \sum_{t_i=t_0}^{t_k} \Delta CMC^i_{if}(t_i) \quad \text{where } t_k = t \tag{9}$$

Consecutive multipath estimation using GNSS CMC variation is summarized as follows. First, an ionosphere-free (IF) measurement is genarated by a linear combination of dual frequency measurements. Next, an initial multipath estimate is computed from the IF pseudorange measurement based on the initial position. Because the IF CMC variation is mainly caused by multipath variation, the multipath is computed from the sum of the initial multipath estimate and the CMC cumulative variation.

B. Compensation for Time Offset Between Constellations

Another serious problem that hinders the availability of urban GNSS navigation as much as multipath errors is the low visibility of GNSS satellites. Because skyscrapers in a city diminish the visibility of GPS satellites, multi-constellation GNSS solutions are essential for the continuous navigation of vehicles in deep urban areas. Navigation availability increases as more satellites are visible, but this increment is not perfectly proportional to the number of visible satellites. GNSS inherently depends on precise timekeeping; therefore, each ground segment makes a significant effort to maintain a highly stable atomic timescale. Nevertheless, clock differences between the constellations continue to exist among the timescales at the level of tens or hundreds of nanoseconds [44]; thus, at least two more satellites should be added to improve the availability of multi-constellation GNSS positioning. For example, when a user cannot obtain the position solution owing to the visibility of three GPS satellites, an additional satellite in GLONASS or other constellations does not help the user, because the dimension of the state has increased from four to five owing to the inter-system bias (ISB).

Incorporating two additional satellites per constellation remains a challenge in deep urban areas. To increase the accuracy by mitigating the multipath errors and availability by adding a constellation, this study proposes the inclusion of ISB into the initial multipath estimates. If the initial multipath and its variation are estimated based on the GPS system clock, multi-constellation positioning is possible with only four satellites, regardless of the number of constellations used for the positioning. As shown in (10), as shown at the bottom of the next page, other systems do not use the same time reference as GPS, and thus an ISB between the other GNSS and GPS, denoted as δB_{GNSS} in (11), arises. where the superscripts I and J refer to the GPS and non-GPS GNSS constellation satellite set, respectively.

$$B_{GNSS^J}(t) = B_{GPS}(t) + \delta B_{GNSS^J}(t) \tag{11}$$

Receivers using measurements from two or more systems need to cope with this time offset; thus, the minimum number of visible satellites should be increased by the number of added constellations to compensate for the difference in clock error [45]. For this multi-constellation GNSS solution($\vec{x}_{GNSS}$), the navigation matrix H_{GNSS} and measurement vector $\vec{z}_{GNSS}$ should be described as shown in (12), where $\vec{e}$ is the LOS unit row vector from the user to each GNSS satellite($\vec{X}$) and $\vec{v}_{GNSS}$ is residual vector for the multi-constellation GNSS solution.

$$\vec{z}_{GNSS} = H_{GNSS}\vec{x}_{GNSS} + \vec{v}_{GNSS} \tag{12}$$

where

$$\left.\begin{aligned}\vec{z}_{GNSS} &= \begin{bmatrix} \vec{e}^{\,i}_{GPS}\cdot\vec{X}^i - \hat{b}^i_{if} + \hat{T}^i + \hat{M}^i_{if} - \rho^i_{if} \\ \vdots \\ \vec{e}^{\,j}_{GLONASS}\cdot\vec{X}^j - \hat{b}^j_{if} + \hat{T}^j + \hat{M}^j_{if} - \rho^j_{if} \\ \vdots \\ \vec{e}^{\,k}_{BeiDou}\cdot\vec{X}^k - \hat{b}^k_{if} + \hat{T}^k + \hat{M}^k_{if} - \rho^k_{if} \\ \vdots \end{bmatrix} \\ H_{GNSS} &= \begin{bmatrix} \vec{e}^{\,i}_{GPS} & 1\,0\,0 \\ \vdots & \vdots\ \vdots\ \vdots \\ \vec{e}^{\,j}_{GLONASS} & 0\,1\,0 \\ \vdots & \vdots\ \vdots\ \vdots \\ \vec{e}^{\,k}_{BeiDou} & 0\,0\,1 \\ \vdots & \vdots\ \vdots\ \vdots \end{bmatrix} \\ \vec{x}_{GNSS} &= \begin{bmatrix} x \\ y \\ z \\ B_{GPS} \\ B_{GLONASS} \\ B_{BeiDou} \end{bmatrix}\end{aligned}\right\}$$

where x, y, and z are geocentric coordinates, B_{GPS}, $B_{GLONASS}$, and B_{BeiDou} are receiver clock bias of GPS, GLONASS and BeiDou, respectively. The estimate of each term is denoted as $\hat{}$.

In the deep urban areas targeted by this study, extremely few GNSS satellites are visible, even when all the available constellations are used. Regardless of its accuracy, multipath estimation is useless if the GNSS position cannot be solved. Because the ISB estimates vary with the data processing center and station as well as the processing time [46], the estimates with 50 ns error is not practically beneficial to both compensating ISB and improving the urban positioning accuracy.

Therefore, if δB_{GNSS} is included in the multipath estimation process, multi-constellation navigation availability is improved, as is its accuracy due to multipath mitigation. To utilize this algorithm, δB_{GNSS^J} should be added to $\hat{M}^j_{if}$, and the multipath estimates of GNSSs other than GPS with reference to GPSTime, $\hat{M}^j_{if|GPST}$, can be obtained as shown in (13).

$$\hat{M}^j_{if|GPST}(t) = \hat{M}^j_{if}(t) + \delta B_{GNSS^J}(t) \tag{13}$$

The multipath estimate at the first epoch referenced to GPSTime, $\hat{M}^j_{if|GPST}(t_0)$, is easily calculated by inserting $B_{GPS}(t_0)$ into (5) instead of $B_{GNSS}(t_0)$ of each constellation system, as described in (14).

$$\begin{aligned}\hat{M}^j_{if|GPST}(t_0) \approx{}& \rho^j_{if}(t_0) - \hat{d}^j(t_0) \\ &- \left(\hat{B}_{GPS}(t_0) - \hat{b}^j_{if}(t_0)\right) - \hat{T}^j(t_0)\end{aligned} \tag{14}$$

Note that because each GNSS maintains a highly stable timescale, $\delta B_{GNSS}(t)$ changes very slowly, typically in the order of femtoseconds per second [45], and we can assume that the ISB between t_0 and t is constant [47]. Although the variation in δB_{GNSS} from t_0 to t is negligible for maneuvering general vehicles, CMC is also referenced by GPSTime to avoid any unexpected divergence. Now, the multipath estimate equation of the non-GPS satellite at time t is changed from (9) to (15).

$$\hat{M}^j_{if|GPST}(t_k) = \hat{M}^j_{if|GPST}(t_0) + \sum\nolimits_{k=t_0}^{t_k} \Delta CMC^j_{if|GPST}(t_i) \tag{15}$$

where $t_k = t$

When a receiver applies the multipath estimates of the i-th GPS and j-th non-GPS satellites to its measurements simultaneously, it can compensate for the ISB while mitigating the multipath errors, as described in (16).

$$\left.\begin{aligned}\rho^i_{if}(t) - \hat{M}^i_{if}(t) - \hat{T}^i + \hat{b}^i &\approx d^i(t) + B_{GPS}(t) \\ \rho^j_{if}(t) - \hat{M}^j_{if|GPST}(t) - \hat{T}^j + \hat{b}^j &\approx d^j(t) + B_{GPS}(t)\end{aligned}\right\} \tag{16}$$

All the pseudoranges in (16), unlike those in (10), are synchronized to GPSTime, and it enables the shrinking of the observation matrix of (12) to that of (17), shown at the bottom of the next page. The GPSTime-synchronized navigation equation including the observation matrix of (17) requires only four visible satellites even when using a multi-constellation, which is expected to enlarge the navigation availability and is therefore suitable for urban areas.

Compensation for time offset between constellations is summarized as follows. To improve both accuracy and availability by maintaining the minimum number of visible satellites for the multi-constellation GNSS solution as four, the initial multipath error is estimated by being referenced to GPSTime. Next, the multipath estimates referenced to GPSTime can be obtained by summing of the initial multipath estimate referenced to GPSTime and the CMC cumulative variation. When the user applies the estimate, both multipath and ISB are eliminated, and the GPSTime-synchronized navigation equation enables multi-constellation GNSS positioning with only four visible satellites.

C. Consecutive CMC-Based Multipath Estimation

The multipath estimation algorithm described above is effective under the assumption that the integer ambiguity remains constant. To check if the algorithm can be continuously available for current measurements, a cycle-slip detection technique was applied to two consecutive carrier phases. The TD of the geometry-free combination of the dual-frequency carrier measurements was used as a cycle-slip

$$\left.\begin{aligned}\rho^I_{if}(t) &= d^I(t) + \left(B_{GPS}(t) - b^I(t)\right) + T^I(t) + M^I_{if}(t) + \epsilon^I_{if}(t) \\ \rho^J_{if}(t) &= d^J(t) + \left(B_{GNSS}(t) - b^J(t)\right) + T^J(t) + M^J_{if}(t) + \epsilon^J_{if}(t)\end{aligned}\right\} \tag{10}$$

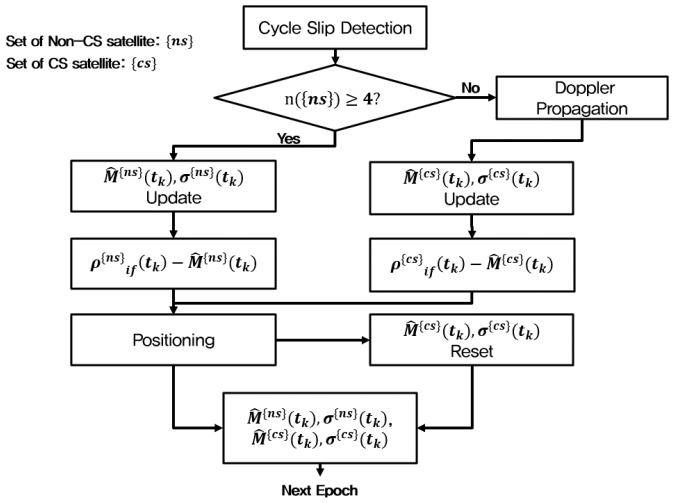

Fig. 1. Consecutive estimation process of CMC-based multipath and its standard deviation.

detection metric, as shown in (18).

$$\Delta I^i_{L1}(t) = \frac{\Delta\phi^i_{L1}(t) - \Delta\phi^i_{L2}(t)}{\gamma - 1} + \frac{[\Delta N_{L2}\lambda_{L2}(\mathrm{t}) - \Delta N_{L1}\lambda_{L1}(\mathrm{t})]}{\gamma - 1} \quad (18)$$

Because ionospheric variation in time is less than 2 cm/s in the mid-latitude region [48], the metric in (18) being larger than the normal value means that the TD of the integers, ΔN_{L1} or ΔN_{L2}, is not zero due to the cycle slip. Fig. 1 describes the process of multipath estimation when cycle slips are found in the current satellite measurements.

Once a cycle-slip alarm is flagged for a satellite at time t_k, the consecutive multipath estimation algorithm is no longer valid for the detected satellite $\{cs\}$.Consecutive multipathestimates for the non-slipped satellites $\{ns\}$ are valid; thus, the position solution at time t_k is still reliable owing to the exclusion of the slipped satellite from the solution, provided the number of non-slipped satellites $n(\{ns\})$ is four or more. Because the position obtained after mitigating the multipath and ionospheric errors for the non-slipped satellites by using (3) and (16) is reliable, the multipath estimate of the slipped satellite $\hat{M}^{\{cs\}}_{if|GPST}$ can be initialized again based on the obtained position using (14).

Recalling the estimate equation of (15), the error variance of the CMC-based multipath estimates, $\left(\sigma^i_{\hat{M}}\right)^2$, is the sum of the first estimate's variance and accumulated variance of the CMC TD, as described in (19). From (6), the CMC includes code noise as well as multipath error in the pseudorange. The code noise and multipath are removed together when $\hat{M}^i_{if}$ estimated by the accumulated CMC is subtracted according to (16), and the variation in the carrier phase residual error is accumulated. The TD of the carrier phase measurement has a millimeter-level residual, which is known to be more accurate than the centimeter-level residual of Doppler [49], [50]. Here, $\sigma^i_{\Delta CMC_{if}}$ was set to 3 cm/s owing to inflation due to the dual frequency combination of carrier phase noise of several mm [51]. Therefore, the uncertainty increases with time after the multipath estimation is initialized.

$$(\sigma^i_{\hat{M}_{if}}(t_k))^2 = (\sigma^i_{\hat{M}_{if}}(t_0))^2 + \sum\nolimits_{t_{i=t_0+\Delta t}}^{t_k} (\sigma^i_{\Delta CMC_{if}}(k)\,\Delta t)^2 \quad \text{where } t_k = t \quad (19)$$

where σ is the standard deviation (std) of each error denoted by the subscript, and Δt is the sampling time.

If the number of available satellites is less than four due to cycle slip and low-visibility, dual-frequency carrier phase measurements should be replaced by ionosphere-free (if) combined Doppler measurements$(d\rho)$ in (20) to extend the if carrier measurement at the previous epoch, as shown in (21). When the Doppler measurements were used, $\sigma^i_{\Delta CMC_{if}}$

$$\left.\begin{aligned} \vec{z}_{GNSS|GPST} &= \begin{bmatrix} \vec{e}^i_{GPS}\cdot\vec{X}^i - \hat{b}^i_{if} + \hat{T}^i + \hat{M}^i_{if} - \rho^i_{if} \\ \vdots \\ \vec{e}^j_{GLONASS}\cdot\vec{X}^j - \hat{b}^j_{if} + \hat{T}^j + \hat{M}^j_{if|GPST} - \rho^j_{if} \\ \vdots \\ \vec{e}^k_{BeiDou}\cdot\vec{X}^k - \hat{b}^k_{if} + \hat{T}^k + \hat{M}^k_{if|GPST} - \rho^k_{if} \\ \vdots \end{bmatrix} \\ H_{GNSS|GPST} &= \begin{bmatrix} e^i_{GPS} & 1 \\ \vdots & \vdots \\ e^j_{GLONASS} & 1 \\ \vdots & \vdots \\ e^k_{BeiDou} & 1 \\ \vdots & \vdots \end{bmatrix} \\ \vec{x}_{GNSS|GPST} &= \begin{bmatrix} x \\ y \\ z \\ B_{GPS} \end{bmatrix} \end{aligned}\right\} \quad (17)$$

was inflated to 30 cm/s [52].

$$d\rho_{if}^{\{cs\}}(t) = \frac{d\rho_{L1}^{\{cs\}}(t) \cdot \gamma - d\rho_{L2}^{\{cs\}}(t)}{\gamma - 1} \tag{20}$$

$$\phi_{if}^{\{cs\}}(t) = \phi_{if}^{\{cs\}}(t - \Delta t) + \frac{d\rho_{if}^{\{cs\}}(t) + d\rho_{if}^{\{cs\}}(t - \Delta t)}{2} \tag{21}$$

After solving the rover's position at time t, the multipath estimates and their uncertainties for the slipped satellites, $\hat{M}_{if|GPST}^{\{cs\}}$ and $\sigma_{M_{if}}^{\{cs\}}$, are initialized.

Consecutive estimation process of CMC-based multipath is summarized as follows. First, cycle slip detection is conducted to check the validity of two consecutive carrier phases. If more than four satellites are available, multipath estimates can be updated by CMC variation and the multipath errors of other invalid but visible satellites are initialized based on the updated position. If there are less than four available satellites due to cycle-slip, the TD of carrier phase is replaced with the Doppler measurement, and then the multipath estimate is updated using the Doppler-based CMC variation.

III. Mode-Switching and Positioning Methodology

A. DGNSS Validation Test

To implement the consecutive multipath estimation process, two problems should be solved in advance: how to determine the initial position and whether the initial position is reliable. DGNSS, which is accurate and reliable code-based GNSS technique, has an accuracy of 1 m. However, there is no way to confirm whether the currently obtained position is reliable without the addition of a camera or 3D map. Instead of adding extra sensors or geographical information, a DGNSS validation test based on residuals was utilized in this study.

The least-square residual vector ($\vec{v}_{DGNSS}$) for the DGNSS solution $\vec{x}_{DGNSS}$ can be expressed as (22), and the corresponding covariance matrix for the DGNSS covariance matrix $P_{\vec{x}_{DGNSS}}$ is described in (23).

$$\vec{v}_{DGNSS} = \vec{z}_{DGNSS} - H\vec{x}_{DGNSS} \tag{22}$$

$$P_{\vec{v}_{DGNSS}} = R - HP_{\vec{x}_{DGNSS}}H^T \tag{23}$$

where $\vec{z}_{DGNSS}$ represents the measurement vector of the corrected pseudorange ($\tilde{\rho}$) after applying the pseudo-range correction (PRC) calculated from the reference station to the raw measurement (ρ), as shown in (24) [53] [54].

$$\left.\begin{aligned} \tilde{\rho}^i &= \rho^i + PRC^i \\ PRC^i &= -\left(-b^i + I^i + T^i\right) = \hat{d}_r^i - \rho_r^i + \hat{B}_r \end{aligned}\right\} \tag{24}$$

where r indicates the reference station.

Under the open sky, most bias errors such as satellite-related and atmospheric errors are mitigated by feeding the PRC to the code observables. The non-differentiated errors of noise and multipath are close to white noise under normal signal reception environments with deviations dependent on the elevation angle(el) [53]. Assuming that there is no correlation between the satellites, non-differentiated error covariance matrix R is given by (25).

$$R = diag\left(\sigma_{DGNSS}^{i\,2}\right) \tag{25}$$

where σ_{DGNSS}^i is the std of z for the i-th satellite in (22). It is the sum of multipath at rover side (rv) and code noise of both the reference station (rs) and rover, as shown in (26). The multipath (σ_m) and noise error (σ_n) models defined for the normal conditions in RTCA standard [55] were used, and we assumed that the multipath can be negligible at the reference station.

$$\sigma_{DGNSS}^i = \sqrt{\sigma_{m,rv}^2\left(el^i\right) + \sigma_{n,rv}^2\left(el^i\right) + \sigma_{n,rs}^2(el^i)} \tag{26}$$

where $\begin{cases} \sigma_m(el) = 0.15 + 0.43e^{-el/6.9^\circ} \\ \sigma_n(el) = 0.13 + 0.53e^{-el/7.5^\circ} \end{cases}$

When the residuals of (22) are sufficiently normal to make the assumption of the zero-mean Gaussian distribution valid, the weighted square sum of error ($WSSE$) of the DGNSS residuals obeys the chi-square distribution (χ^2) with k degrees of freedom. As the residuals are dependent on the 3-dimensional coordinate and system clock, the degrees of freedom k is described in (27).

$$k = n(\{sv\}) - n(\{cst\}) - 3 \tag{27}$$

where $n(\{sv\})$ and $n(\{cst\})$ are the number of satellites used for DGNSS and the number of constellations used for DGNSS, respectively. However, if any instance of $\hat{v}$ contains a mix of biases, mostly due to the multipath error in urban areas, the $WSSE$ becomes too large to follow the χ^2 distribution [56]. Thus, $WSSE$ in (28) can represent the multipath detection function and it can be used to determine the current rover's signal reception environment.

$$WSSE = \vec{v}_{DGNSS}{}^T P_{\vec{v}_{DGNSS}}{}^{-1}\vec{v}_{DGNSS} \tag{28}$$

According to the Neyman–Pearson criterion, when the false alarm rate α is determined, the threshold T_d is determined by solving the equation $P(WSSE > T_d) = \alpha$ [57]. Here, we set the false-alarm rate to 0.01%.

Therefore, it can be considered that all the GNSS signals have been received in suburban or open-sky areas if $WSSE$ passes the chi-square test in (28). Because the current DGNSS solution is reliable, all multipath estimates can be initialized, and the CMC-based multipath process is ready to start.

Conversely, if $WSSE$ is greater than T_d, some of the visible satellites are suspected to be severely corrupted due to multipath in the urban area, and the DGNSS result is no longer reliable. It is difficult to apply the widely used RAIM method because the number of satellites that are seriously affected by the multipath is unknown. However, the proposed algorithm can estimate the multipath errors continuously from the initial position regardless of the number of satellites that are corrupted by multipath and the source of the multipath error (LOS or NLOS). Therefore, the rover can determine its accurate position by effectively mitigating all multipath errors,

even in a deep urban area.

$$\begin{cases} WSSE > T_d & \text{severemultipath(SM)} \\ WSSE \leq T_d & \text{multipath} - \text{free(MF)} \end{cases} \tag{29}$$

Even without any camera or building information, the rover can determine whether there are any obstacles that cause multipath based on the signal reception decision criterion of (29). Because the final positioning algorithm depends on the signal reception environment, it is used as the positioning mode-switching criterion, which is explained in the next section.

B. Positioning Mode-Switching Algorithm

Once the signal reception decision criterion determines that the rover is currently under a "severe multipath (SM) environment," the DGNSS position is no longer valid. The current position should be computed after mitigating the multipath by using the suggested estimation algorithm until the environment is changed to "multipath-free (MF)" because of a change in the rover's maneuvering or satellite geometry. Although the recursively estimated multipath improves the position accuracy of urban users using (17) and (18), the uncertainty gradually increases owing to the accumulation of the carrier phase TD or Doppler, as shown in (19). The uncertainty does not increase with the same magnitude because the initialization time is different for each satellite; however, the noise covariance model for the measurements in the SM environment in (30), $R_{\vec{z}_{SM}}$, increases in proportion to time. Consequently, the SM mode positioning error covariance $P_{\hat{\vec{x}}_{SM}}$ inevitably increases. Therefore, it is risky to run the multipath estimation filter over a long period from the initial multipath-fix time.

$$R_{\vec{z}_{SM}}(t) = diag\left\{\left(\sigma^i_{\hat{M}_{if}}(t)\right)^2 + \left(\sigma^i_{n,rs}(t)\right)^2\right\} \tag{30}$$

The moment when the multipath environment is switched from SM to MF is a good opportunity to renew the initialization time. Unlike the SM condition, the DGNSS position $\vec{x}_{DGNSS}$ and multipath-mitigated position $\hat{\vec{x}}_{SM}$ can be both valid in the MF environment. By combining two valid positions, $\vec{x}_{DGNSS}$ and $\hat{\vec{x}}_{SM}$, based on their estimated error covariances $P_{\vec{x}_{DGNSS}}$ and $P_{\hat{\vec{x}}_{SM}}$, the optimal position for the MF mode can be estimated as (31).

$$\left.\begin{aligned} \hat{\vec{x}}_{MF}(t) &= P_{\hat{\vec{x}}_{MF}}(t)\left(P^{-1}_{\vec{x}_{DGNSS}}(t)\vec{x}_{DGNSS}(t) + P^{-1}_{\hat{\vec{x}}_{SM}}(t)\hat{\vec{x}}_{SM}(t)\right) \\ P_{\hat{\vec{x}}_{MF}}(t) &= \left(P^{-1}_{\vec{x}_{DGNSS}}(t) + P^{-1}_{\hat{\vec{x}}_{SM}}(t)\right)^{-1} \end{aligned}\right\} \tag{31}$$

IV. Field Test in Deep Urban Area and Results

A. Field Test Construction

To verify the applicability of the algorithm to actual deep urban areas, a field test was performed along Teheran-ro, Seoul, Korea, which is one of the streets with the poorest GNSS visibility and signal reception globally. Fig.2 shows the GNSS visibility of Teheran-ro. According to the analysis

Fig. 2. Deep urban canyons in Teheran-ro (Seoul, South Korea).

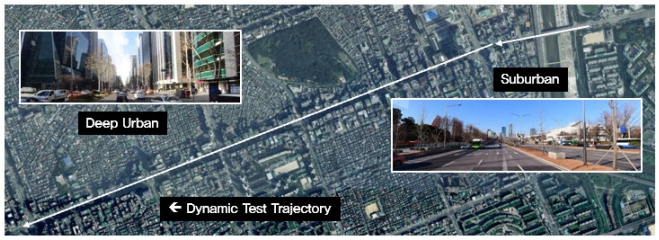

Fig. 3. Dynamic test trajectory.

based on the 3D building information in this area, only 2.5 GPS satellites are visible on average and GPS-only positioning is available for 20% of the day [58]. Although this area is within the "GNSS satellite hotspot," [59] where all constellation signals in operation are available, only 4 satellites are visible despite using all the constellations, and the multi-GNSS position is not available for approximately 10% of the day [60]. The low visibility and availability result in positioning vulnerable to multipath and poor accuracy. The average position error RMS in this area was reported to be 55.6 m due to the significant effect of multipath [61].

The dynamic test trajectory, which included Teheran-ro, is shown in Fig. 3. The starting point was a relatively suburban area, but most of the driving was on the road in the middle of a deep urban area. There was a bridge at the border between the suburban area near the starting point and the deep urban area, in which all signals were blocked before entering the urban area.

For the dynamic field test, a vehicle equipped with a GNSS receiver and reference system was used, as shown in Fig. 4. A NovAtel FlexPak6 GNSS receiver was used to receive the GPS/GLONASS/BeiDou dual-frequency pseudorange and carrier phase measurements, and NovAtel SPAN-CPT provided a continuous 3D true reference trajectory even when signal reception was briefly compromised. The GNSS signal recorder LabSat 3 was also mounted with other devices to acquire the position results to be compared by reradiating the same signals to other modes of the receiver.

The test was carried out for approximately half an hour from 7:40 to 8:10 UTC on September 14, 2019. Fig. 5 shows the satellite visibility during the dynamic test. The average number of available GPS satellites was 3.74 during the dynamic test, and the average number of available satellites was

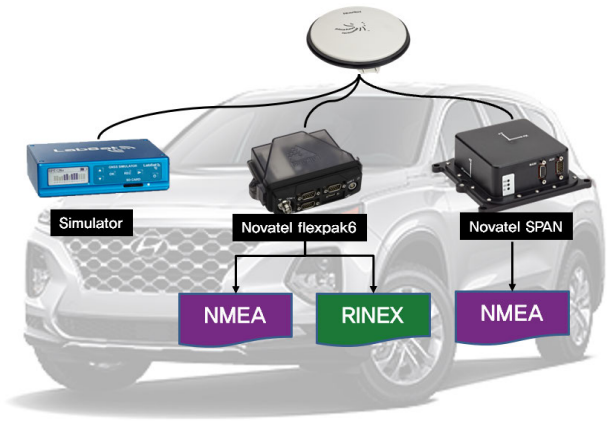

Fig. 4. Dynamic test configuration.

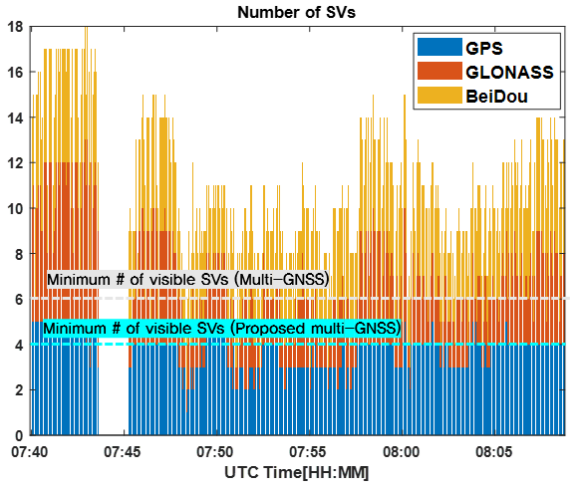

Fig. 5. Satellite visibility during dynamic test.

10.8 even after adding two more constellations, GLONASS and BeiDou. The average number of available GPS satellites was 3.74 during the test, which provided GPS-only position for 35.6% of the period. Adding GLONASS and Beidou to GPS-only was effective in improving the availability of the conventional multi-constellation GNSS positioning up to 99%. However, the conventional method was ineffective for 30 sec, 1% of period including 07:48:21–07:48:25, 07:51:00–07:51:04 despite adding two constellations. In contrast, the proposed method of mitigating multipath with ISB compensation enabled the urban positioning availability to be 100% throughout the test. In addition, the redundancy of available satellites became higher than that of the conventional methods, which can improve position accuracy and system robustness.

B. Field Test Results

The multipath error for all visible satellites estimated on Teheran-ro according to the algorithm described in Section II is shown in Fig. 6. One notable aspect is that there are two groups of estimates with values centered at 0 and 30 m. The estimates mainly clustered at 30 m are the multipath errors of the BeiDou satellite, which were estimated by referring to the GPSTime and not the BeiDou time according to (14).

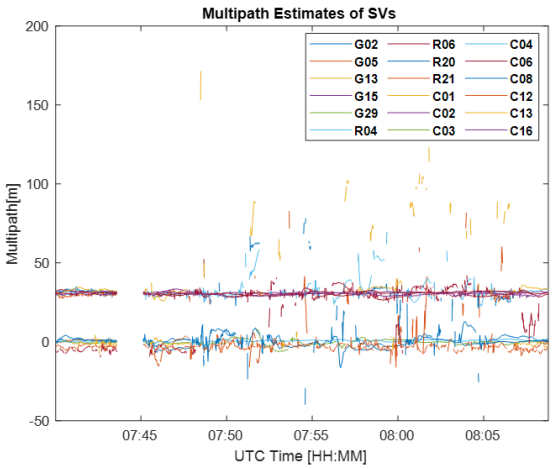

Fig. 6. Estimated multipath of multi-constellation satellites.

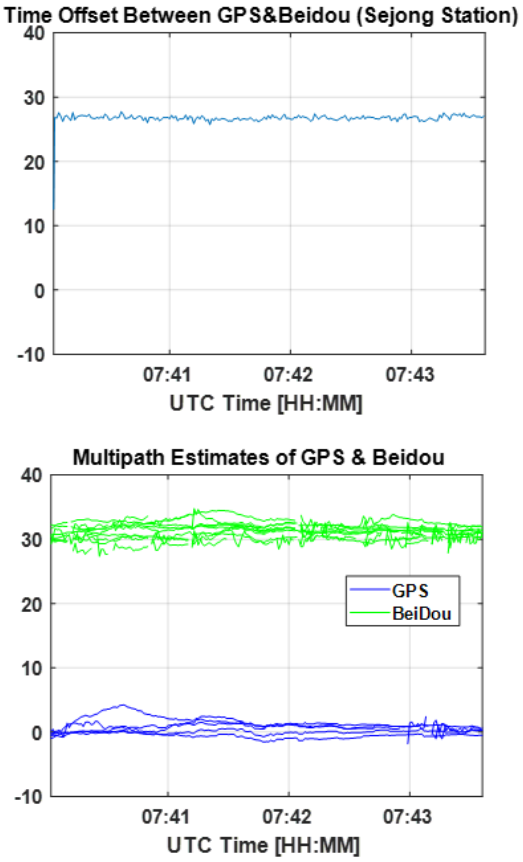

Fig. 7. Estimated time offset between GPS and BeiDou.

This means that the clock offset between GPS and BeiDou was approximately 30 m (≈100 ns) during the dynamic test, as shown in Fig. 7. The clock offset between GPS and BeiDou computed under the open sky at the Sejong University reference station (Fig. 7, top) was similar to the estimated bias calculated (Fig. 7, bottom) using the suggested technique during the dynamic test in the deep urban area.

Considering the bias due to the clock offset between the systems, a large number of real multipath errors were estimated to be less than 50 m, but some were larger than 150 m, which confirms that NLOS multipath were included in the measurements. Thus, the proposed algorithm

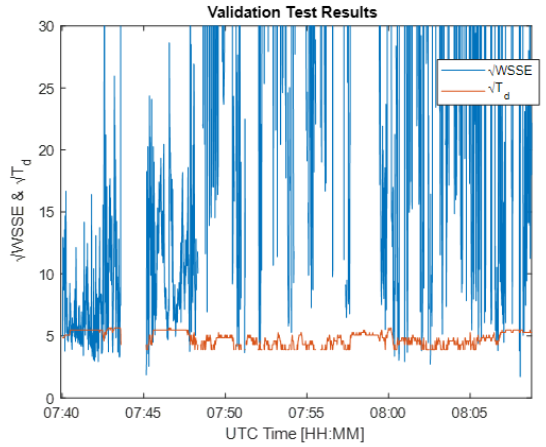

Fig. 8. DGNSS residual validation test results.

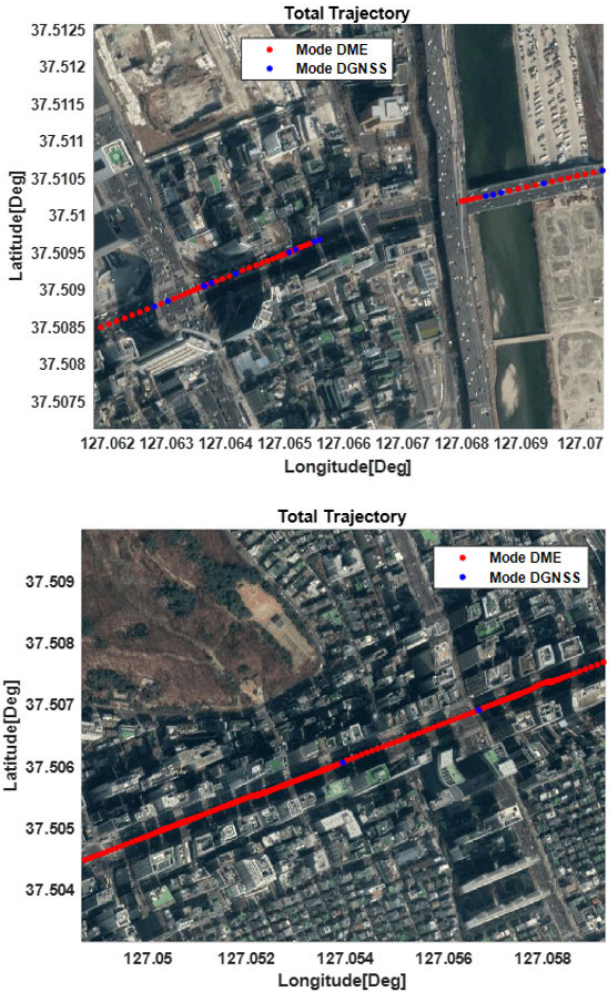

Fig. 9. SM and MF points in test area (top: sub-urban, bottom: deep urban).

can estimate the multipath error regardless of whether it is LOS or NLOS. The estimates are highly discrete because the vehicle movement constantly changes the satellite geometry and surrounding buildings. In this study, in order to evaluate how well the multipath estimates mitigate the actual errors, all visible satellites were used for positioning without applying a satellite exclusion technique such as RAIM.

The rover can detect if the vehicle is currently driving in the SM or MF environment based on the signal reception decision criterion of (26) without additional sensors or information. According to our test results in Fig. 8, the DGNSS positions were acceptable for only 6% of the dynamic test. The points judged as MF were mostly located at the starting and ending points in relatively suburban areas. In urban areas from 7:45 to 8:08 UTC, the $WSSE$s at most points were calculated to be larger than T_d; therefore, the DGNSS results were mostly unreliable. However, the DGNSS results at 31 points among them were determined to be calculated in MF environments, which are marked on the maps in Fig. 9. As all these points were located near intersection points where relatively good satellite visibilities were provided, it can be concluded that this criterion was valid for determining the signal reception environment.

These DGNSS-valid points within urban canyons prevent the divergence of positioning error by stopping the uncertainty accumulation in each measurement considered in (19). The functionalities of these points in the measurement and position domains are presented in Fig. 10, especially in the dotted box magnified for the duration from 07:48 to 08:03. As shown in the map of Fig. 9, the horizontal dilution of precision (HDOP) at those points was temporarily very low when compared with the other points because the criterion of (27) identified sites that provided good visibility. At these points, $\hat{\vec{x}}_{MF}$ is computed by optimizing $\vec{x}_{DGNSS}$ and $\hat{\vec{x}}_{SM}$, and its error covariance $P_{\hat{\vec{x}}_{MF}}$ is significantly reduced from $P_{\hat{\vec{x}}_{SM}}$ accumulated until the previous epoch, as shown in the third row. Based on the reliable MF position $\hat{\vec{x}}_{MF}$, all the multipath estimates $\hat{M}^j_{if|GPST}$ were initialized, and their stds were reduced to the initial values. Because there was no valid DGNSS result from 7:51:11 to 8:00:34 UTC, the multipath error was continuously estimated without initialization, and the uncertainty for all the satellites was accumulated, as shown in the magnified box of Fig. 10.

The DGNSS result was finally determined to be valid at 7:51:11 UTC, and the multipath estimates for all the satellites were initialized and fixed based on the reliable position that resulted in reduced std. The variation in the position error modeling was similar to that of the measurement. Because the combined positions accuracy of the DGNSS and SM position is expected to be accurate and reliable, these points in the deep urban areas significantly contribute to reducing the position error accumulation and divergence to an incorrect position. The multipath estimation based on the synchronization to GPSTime greatly contributed to improving the availability. Fig. 11 shows a skyplot snapshot at the 507th epoch, when five satellites in three constellations, namely, GPS, GLONASS, and BeiDou, were visible. Because GLONASS and BeiDou are operated based on their own clock systems, two more state variables, i.e., a total of six variables, are necessary for the general multi-GNSS positioning techniques. The conventional multi-GNSS positioning definitely could not compute the position, but the algorithm in this study could solve it with one redundancy because it required only four variables in the solution state owing to the elimination of the ISB. This example clearly demonstrates that the proposed method is

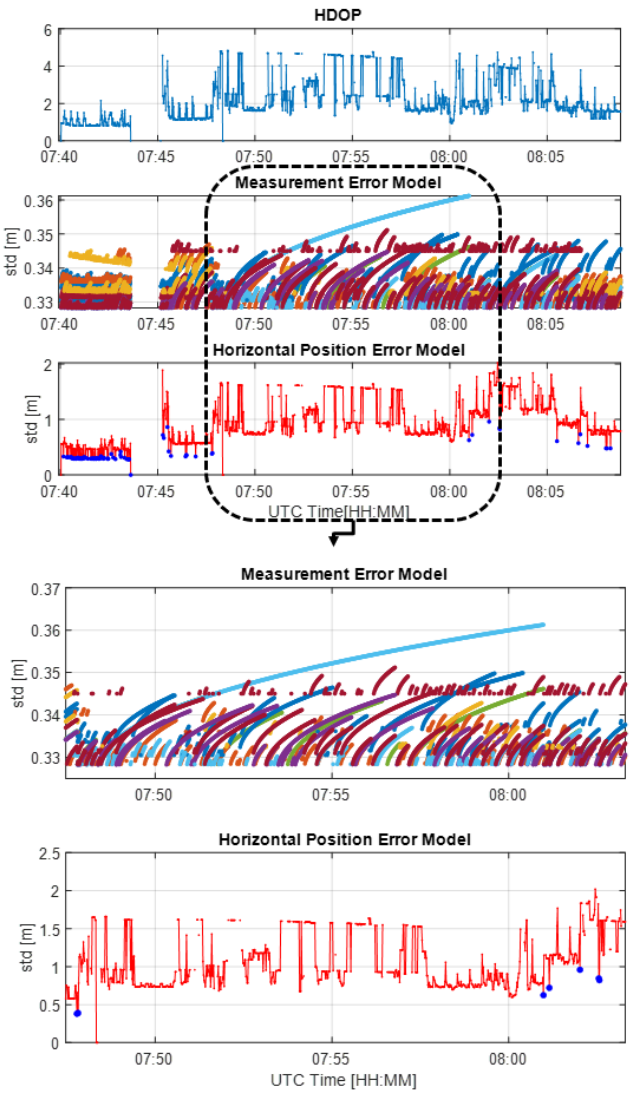

Fig. 10. HDOP and error model std variation in measurement and position domains.

suitable for improving position availability in deep urban areas where satellite visibility is very limited.

Doppler-based multipath estimation propagation complements CMC-based estimation under the condition of low visibility of satellites. Because the TD of the carrier observable is utilized for the CMC-based estimation method, the condition that valid carrier phases must be consecutively measured at the current epoch as well as the previous epoch and the condition of no cycle slip must be satisfied. Fig. 12 shows the point at which the multipath was estimated using the Doppler measurement during the dynamic test and its position error. As shown in Fig. 12, valid consecutive positions were provided by the Doppler propagation, even when the carrier phases of only three satellites were available due to cycle slip.

As described above, the signal reception environment of the rover at each time was identified based on the DGNSS residual test; then, the multi-constellation GNSS multipath errors were mitigated by the GPSTime-synchronized CMC-based consecutive estimation technique for all the tests, and Doppler measurements were used as complementary measurements at the sites with extremely poor availability.

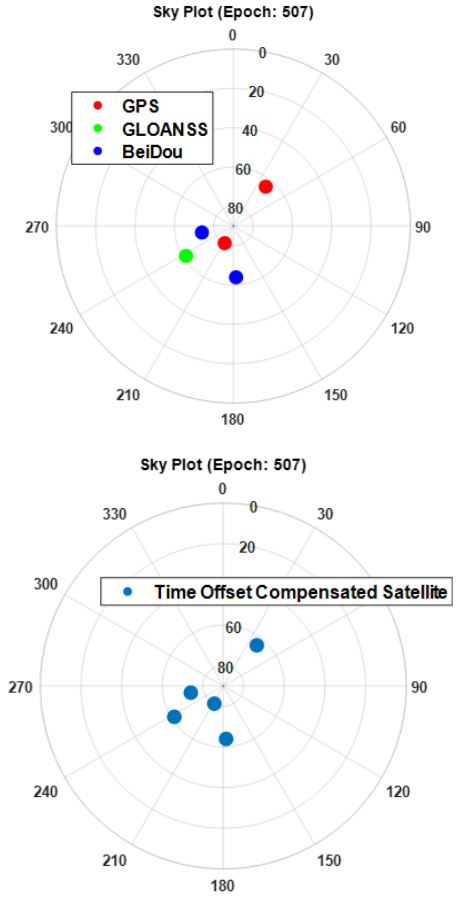

Fig. 11. Multi-constellation satellite geometry (top: conventional multi-GNSS positioning, bottom: GPSTime-synchronized method).

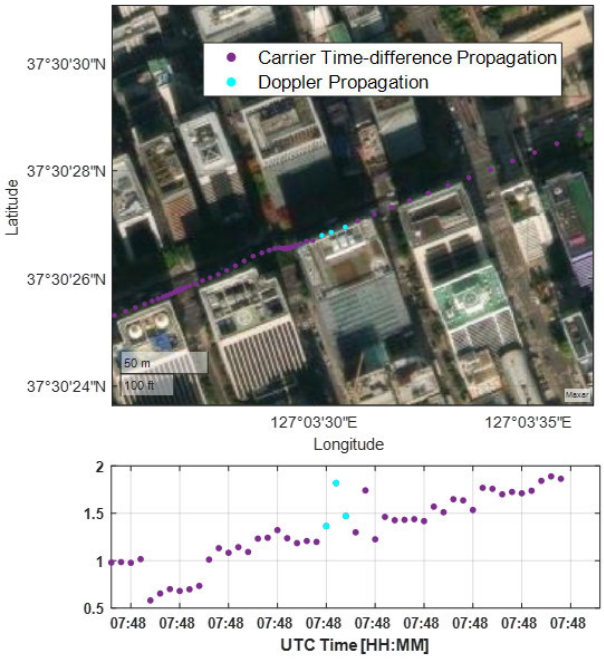

Fig. 12. Position complement by Doppler-based method.

The multipath-mitigated positions of $\hat{\vec{x}}_{SM}$ were combined with $\vec{x}_{DGNSS}$ to determine the final positions in the urban areas. The east-north-up (ENU) error at each time point

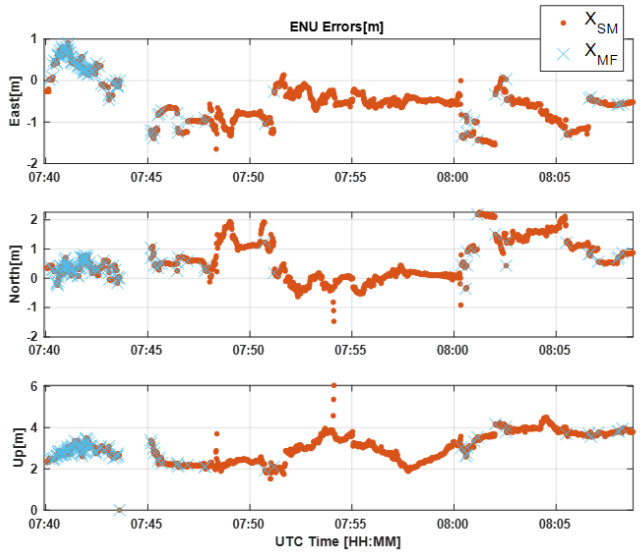

Fig. 13. DGNSS residual validation results.

TABLE II
STATISTICAL RESULTS OF DYNAMIC TEST

Statistical Results		RMS	95%	Max	Availability
Multipath-Free Position	Hor	1.2m	2.3m	2.7m	100%
	Ver	3.0m	4.0m	6.0m	
Flexpak6 DGNSS	Hor	11.1m	15.6m	101.0m	64.8%
	Ver	3.9m	13.7m	127.6m	
Flexpak6 SBAS	Hor	11.3m	25.7m	62.6m	4.2%
	Ver	4.0m	8.6m	17.13m	
Flexpak6 RTK	Hor	14.3m	37.1m	115.0m	0.0%(fixed)
	Ver	11.5m	23.4m	216.6m	40.1%(float)

was computed based on the true trajectory from the SPAN, as shown in Fig. 13. The positions were successfully computed during the entire 30-min dynamic test in Teheran-ro, and the root mean square (RMS) of the horizontal positioning error was computed as 1.2 m. The 95% cumulative error was 2.3 m, and the maximum error was only 2.7 m.

These results are superior to those of other conventional methods in terms of accuracy and availability. The GNSS signals recorded by LabSat-3 during the dynamic test were re-radiated to the NovAtel FlexPak6 in various modes, and real-time DGNSS, satellite-based augmentation system (SBAS), and RTK were replayed using the method presented in our previous study [62], [63]. The trajectory of the suggested method along with those of RTK, DGNSS, and SBAS for the NovAtel receiver is shown in Fig. 14. The availability of the suggested method was 100%, whereas the DGNSS technique could calculate the position for 64.8% of the test section.

In addition to the availability, the RMS error of the proposed method was only approximately 1/10 of that of the DGNSS horizontal results, and the maximum error of over 100 m was reduced to less than 3 m as shown in Fig. 15 and Table II. Because the SBAS correction was applied to only GPS satellites, the receiver in the SBAS mode was able to calculate the position for only 4.2% of the test section. The overall accuracy, i.e., the horizontal RMS, was 11.3 m, as in the case of DGNSS, which has the same code differential positioning. However, the maximum error and 95% error of

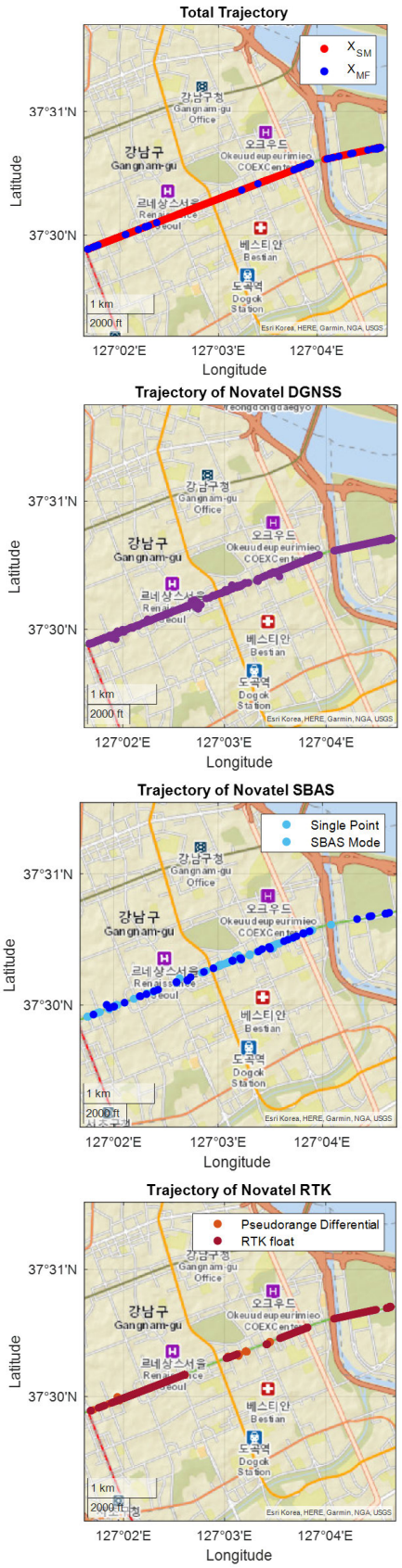

Fig. 14. Position availability comparison for various modes.

SBAS are statistically better than those of DGNSS because SBAS positioning is possible at points with better visibility

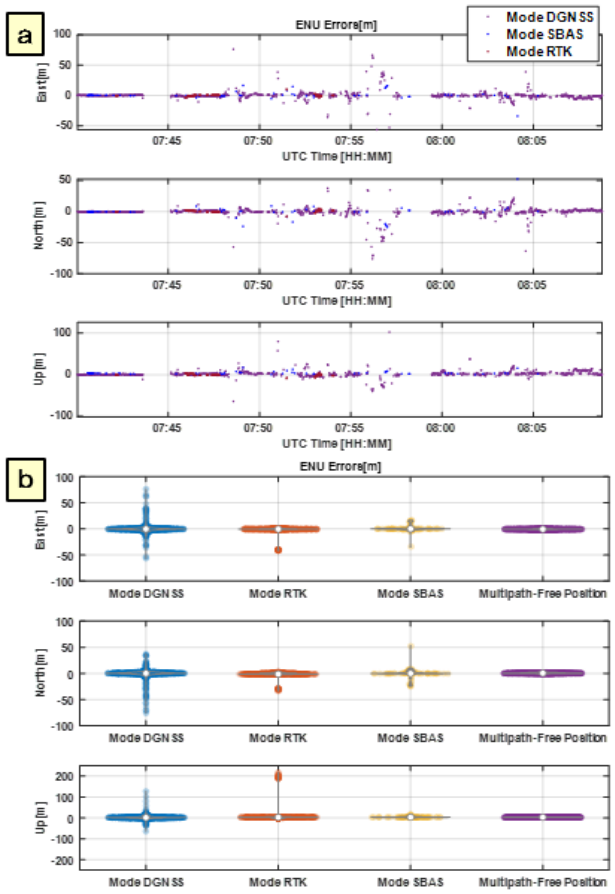

Fig. 15. Position accuracy comparison for various modes ((a) Time history of ENU error, (b) violin plot of ENU error).

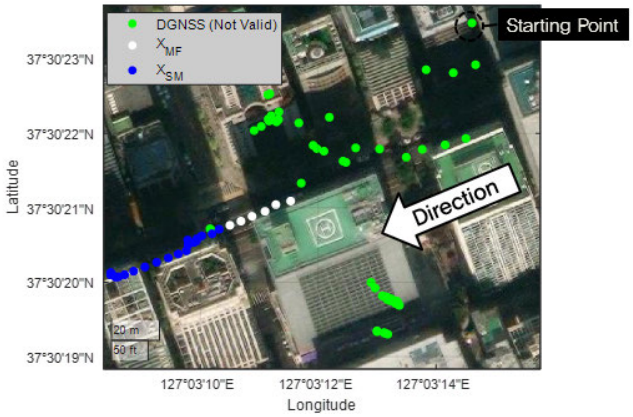

Fig. 16. Proposed algorithm initiated in the middle of urban canyon.

when compared with multi-constellation DGNSS. When the receiver was in the RTK mode, the position was computed in 52.3% of the session, but no positions were computed in the RTK fixed mode whereas the positions were computed for 40% of the session in the RTK float mode. Despite the computation in the RTK float mode, the performance was assessed in terms of the horizontal error RMS instead of the commonly expected cm or dm accuracy; the error was computed to be 14 m, which was larger than the code-based results. The maximum error also reached 115 m horizontally and 216 m vertically; thus, the technique could not take advantage of the carrier-based positioning at all. While the accuracy improvement by the high-end technology summarized in Table I was 60%, the method proposed here could reduce the error by 75%.

V. Conclusion and Future Works

This paper introduced an effective algorithm for mitigating severe multipath to determine the DGNSS positioning accuracy level consistently in deep urban areas without additional sensors or information other than GNSS. The existing methods selectively enhanced either the accuracy or availability, but the suggested method could improve both performance metrics. This method was able to estimate both LOS and NLOS without any algorithm variant, which also distinguishes it from other studies.

To validate the suggested algorithm and demonstrate its performance in urban canyons, we conducted a dynamic test in Teheran-ro, which is known for low visibility of satellites. The half-hour driving test results showed that the proposed algorithm could provide the rover's real-time results for 100% of the session, whereas the conventional method of the commercial receiver calculated the positions for only 64% of the session. The horizontal error RMS of the commercial receiver was 11.1 m, which was reduced to 1.2 m by applying the suggested algorithm to the receiver. From this result, we confirmed that the recognition of the signal reception environment and estimation of the GNSS multipath was valid and adequate to enable 1 m accuracy and 100% availability in a deep urban area.

Because this method does not require any prior information before deployment, it is expected that consistent position performance will be achieved in cities other than Seoul. This technique is easy to implement when only the receiver provides dual frequency measurements; therefore, it is expected that it will be widely used not only in automobiles but also in various future intelligent transportation systems, including smart mobility based on electric bicycles, scooters, and drones.

As a limitation, precise positions can be computed only after the vehicle obtains a reliable initial position such as a valid DGNSS. If the algorithm is initiated in the middle of a deep urban area, the CMC-based multipath mitigation technique would not be initiated till a valid DGNSS position was found and instead return invalid flags. Thus, when the data starts from a dense urban place, the position module issues invalid solution alarms because it skips multipath mitigation. However, it would not last long because the suggested algorithm would keep on seeking a valid initial position for the process initiation. Fig. 16 shows the results of finding a new initial position when data started in the middle of dense urban canyons. The position error at the starting point was approximately 46 m horizontally, and the positions had been invalid marked in green dots till a valid DGNSS position was found. After finding the first valid initial position with horizontal error of 1.7 m, valid DGNSS positions for 6 s marked in white dots initiated the CMC-based multipath mitigation so that the MF positions marked in blue

dots are continuously acquired afterward. Nevertheless, it is important to reduce the invalid period of first 30 s to achieve fully seamless and accurate positioning in deep urban areas. Therefore, our future work will focus on finding an initial accurate position to quickly start this algorithm wherever the data tracking starts in the middle of an urban canyon.

REFERENCES

[1] K. N. Qureshi and A. H. Abdullah, "A survey on intelligent transportation systems," *Middle-East J. Sci. Res.*, vol. 15, no. 5, pp. 629–642, 2013.

[2] R. Hussain and S. Zeadally, "Autonomous cars: Research results, issues, and future challenges," *IEEE Commun. Surveys Tuts.*, vol. 21, no. 2, pp. 1275–1313, 2nd Quart., 2019.

[3] S. Bijjahalli, R. Sabatini, and A. Gardi, "GNSS performance modelling and augmentation for urban air mobility," *Sensors*, vol. 19, no. 19, Sep. 2019, Art. no. 4209.

[4] European GNSS Agency (GSA). (2019). *GSA GNSS Market Report*. [Online]. Available: https://www.gsa.europa.eu/market/market-report

[5] H. Ritchie and M. Roser. (2018). Urbanization. Our World in Data. Accessed: Mar. 20, 2023. [Online]. Available: https://ourworldindata.org/urbanization

[6] C. Rizos, "Trends in GPS technology & applications," in *Proc. 2nd Int. LBS Workshop*, 2003, pp. 1–41.

[7] P. D. Groves, "How does non-line-of-sight reception differ from multipath interference," *Inside GNSS*, vol. 8, pp. 40–42, Nov. 2013.

[8] D. Imparato, A. El-Mowafy, C. Rizos, and J. Wang, "Vulnerabilities in SBAS and RTK positioning in intelligent transport systems: An overview," in *Proc. IGNSS Symp.*, Sydney, NSW, Australia, 2018, pp. 1–17.

[9] F. van Diggelen, "End game for urban GNSS: Google's use of 3D building models," Inside GNSS, 2021.

[10] G. Zhang and L. Hsu, "Performance assessment of GNSS diffraction models in urban areas," *Navigation*, vol. 68, no. 2, pp. 369–389, Jun. 2021.

[11] G. MacGougan et al., "Performance analysis of a stand-alone high-sensitivity receiver," *GPS Solutions*, vol. 6, no. 3, pp. 179–195, 2002.

[12] K. Ali, M. Pini, and F. Dovis, "Measured performance of the application of EGNOS in the road traffic sector," *GPS Solutions*, vol. 16, no. 2, pp. 135–145, Apr. 2012.

[13] J. Marais, M. Berbineau, and M. Heddebaut, "Land mobile GNSS availability and multipath evaluation tool," *IEEE Trans. Veh. Technol.*, vol. 54, no. 5, pp. 1697–1704, Sep. 2005.

[14] L. Wang, P. D. Groves, and M. K. Ziebart, "Smartphone shadow matching for better cross-street GNSS positioning in urban environments," *J. Navigat.*, vol. 68, no. 3, pp. 411–433, 2015.

[15] L. Wang, P. D. Groves, and M. K. Ziebart, "GNSS shadow matching: Improving urban positioning accuracy using a 3D city model with optimized visibility scoring scheme," *Navigation*, vol. 60, no. 3, pp. 195–207, Sep. 2013.

[16] N. Zhu, J. Marais, D. Bétaille, and M. Berbineau, "GNSS position integrity in urban environments: A review of literature," *IEEE Trans. Intell. Transp. Syst.*, vol. 19, no. 9, pp. 2762–2778, Sep. 2018.

[17] S. Bijjahalli, A. Gardi, and R. Sabatini, "GNSS performance modelling for positioning and navigation in urban environments," in *Proc. 5th IEEE Int. Workshop Metrol. Aerosp. (MetroAeroSpace)*, Rome, Italy, Jun. 2018, pp. 521–526.

[18] J. S. Sánchez, A. Gerhmann, P. Thevenon, P. Brocard, A. B. Afia, and O. Julien, "Use of a FishEye camera for GNSS NLOS exclusion and characterization in urban environments," in *Proc. Int. Tech. Meeting Inst. Navigat.*, Monterey, CA, USA, Feb. 2016, pp. 283–292.

[19] T. Suzuki, M. Kitamura, Y. Amano, and T. Hashizume, "High-accuracy GPS and GLONASS positioning by multipath mitigation using omnidirectional infrared camera," in *Proc. IEEE Int. Conf. Robot. Autom.*, Shanghai, China, May 2011, pp. 311–316.

[20] J.-I. Meguro, T. Murata, J.-I. Takiguchi, Y. Amano, and T. Hashizume, "GPS multipath mitigation for urban area using omnidirectional infrared camera," *IEEE Trans. Intell. Transp. Syst.*, vol. 10, no. 1, pp. 22–30, Mar. 2009.

[21] M. Lisi, "GNSS user technology report 2020," *GEOmedia*, vol. 24, no. 5, p. 26, 2020.

[22] T. Qin, P. Li, and S. Shen, "VINS-mono: A robust and versatile monocular visual-inertial state estimator," *IEEE Trans. Robot.*, vol. 34, no. 4, pp. 1004–1020, Aug. 2018.

[23] X. Bai, W. Wen, and L.-T. Hsu, "Robust visual-inertial integrated navigation system aided by online sensor model adaption for autonomous ground vehicles in urban areas," *Remote Sens.*, vol. 12, no. 10, p. 1686, May 2020.

[24] Y. Gu, L.-T. Hsu, and S. Kamijo, "GNSS/onboard inertial sensor integration with the aid of 3-D building map for lane-level vehicle self-localization in urban canyon," *IEEE Trans. Veh. Technol.*, vol. 65, no. 6, pp. 4274–4287, Jun. 2016.

[25] Z. Huan and W. Zunpei, "An INS/GNSS/OD integrated navigation algorithm based on factor graph," in *Proc. IEEE 9th Joint Int. Inf. Technol. Artif. Intell. Conf. (ITAIC)*, Dec. 2020, pp. 2266–2270.

[26] W. Li, X. Cui, and M. Lu, "A robust graph optimization realization of tightly coupled GNSS/INS integrated navigation system for urban vehicles," *Tsinghua Sci. Technol.*, vol. 23, no. 6, pp. 724–732, Dec. 2018, doi: 10.26599/TST.2018.9010078.

[27] W. Wen, T. Pfeifer, X. Bai, and L. T. Hsu, "Factor graph optimization for GNSS/INS integration: A comparison with the extended Kalman filter," *Navigat., J. Inst. Navigat.*, vol. 68, no. 2, pp. 315–331, 2021.

[28] W. Wen, X. Bai, Y. C. Kan, and L.-T. Hsu, "Tightly coupled GNSS/INS integration via factor graph and aided by fish-eye camera," *IEEE Trans. Veh. Technol.*, vol. 68, no. 11, pp. 10651–10662, Sep. 2019.

[29] K. Ali, X. Chen, F. Dovis, D. De Castro, and A. J. Fernández, "GNSS signal multipath error characterization in urban environments using LiDAR data aiding," in *Proc. IEEE 1st AESS Eur. Conf. Satell. Telecommun. (ESTEL)*, Rome, Italy, Oct. 2012, pp. 1–5.

[30] W. W. Wen, G. Zhang, and L.-T. Hsu, "GNSS NLOS exclusion based on dynamic object detection using LiDAR point cloud," *IEEE Trans. Intell. Transp. Syst.*, vol. 22, no. 2, pp. 853–862, Feb. 2021.

[31] A. Abdallah and Z. Kassas, "Multipath mitigation via synthetic aperture beamforming for indoor and deep urban navigation," *IEEE Trans. Veh. Technol.*, vol. 70, no. 9, pp. 8838–8853, Sep. 2021.

[32] P. D. Groves, "Shadow matching: A new GNSS positioning technique for urban canyons," *J. Navigat.*, vol. 64, no. 3, pp. 417–430, Jul. 2011.

[33] Y. Gao, S. Liu, M. A. Mohamed, and A. Noureldin, "INS/GPS/LiDAR integrated navigation system for urban and indoor environments using hybrid scan matching algorithm," *Sensors*, vol. 15, pp. 23286–23302, Sep. 2015.

[34] W. Wen, G. Zhang, and L. Hsu, "Correcting NLOS by 3D LiDAR and building height to improve GNSS single point positioning," *Navigation*, vol. 66, no. 4, pp. 705–718, Dec. 2019.

[35] S. Miura, L.-T. Hsu, F. Chen, and S. Kamijo, "GPS error correction with pseudorange evaluation using three-dimensional maps," *IEEE Trans. Intell. Transp. Syst.*, vol. 16, no. 6, pp. 3104–3115, Jun. 2015.

[36] A. Kumar and A. K. Singh, "A novel multipath mitigation technique for GNSS signals in urban scenarios," *IEEE Trans. Veh. Technol.*, vol. 69, no. 3, pp. 2649–2658, Mar. 2020.

[37] L. Wang, P. D. Groves, and M. K. Ziebart, "Multi-constellation GNSS performance evaluation for urban canyons using large virtual reality city models," *J. Navigat.*, vol. 65, no. 3, pp. 459–476, Jul. 2012.

[38] S. Tay and J. Marais, "Weighting models for GPS Pseudorange observations for land transportation in urban canyons," in *Proc. 6th Eur. Workshop GNSS Signals Signal Process.*, 2013, p. 4.

[39] Z. Jiang and P. D. Groves, "GNSS NLOS and multipath error mitigation using advanced multi-constellation consistency checking with height aiding," in *Proc. 25th Int. Tech. Meeting Satell. Division Inst. Navigat. (ION GNSS)*, Nashville, TN, USA, 2012, pp. 79–88.

[40] A. Pirsiavash, A. Broumandan, G. Lachapelle, and K. O'Keefe, "GNSS code multipath mitigation by cascading measurement monitoring techniques," *Sensors*, vol. 18, no. 6, p. 1967, Jun. 2018.

[41] Y. Lee, B. Park, Y. Hwang, B.-S. Lee, and J. Ahn, "Direct estimation of multipath in a deep urban area using multi-GNSS carrier phase variation and previous position," in *Proc. ION Pacific PNT*, Honolulu, HI, USA, May 2019, pp. 728–736, doi: 10.33012/2019.16835.

[42] J. Kim et al., "A low-cost, high-precision vehicle navigation system for deep urban multipath environment using TDCP measurements," *Sensors*, vol. 20, no. 11, Jun. 2020, Art. no. 3254, doi: 10.3390/s20113254.

[43] J. Saastamoinen, "Contributions to the theory of atmospheric refraction," *Bull. Géodésique*, vol. 105, no. 1, pp. 279–298, Sep. 1972.

[44] R. Shang, C. Gao, W. Gao, R. Zhang, and Z. Peng, "A single difference-based multi-GNSS inter-system model with consideration of inter-frequency bias and inter-system bias," *Meas. Sci. Technol.*, vol. 32, no. 3, Dec. 2020, Art. no. 035013.

[45] M. Petovello, "GNSS solutions: Calculating time offsets," Inside GNSS, 2013.

[46] J. Hong et al., "Characteristics of inter-system biases in multi-GNSS with precise point positioning," *Adv. Space Res.*, vol. 63, no. 12, pp. 3777–3794, Jun. 2019, doi: 10.1016/j.asr.2019.02.037.
[47] I. Vanschoenbeek, B. Bonhoure, M. Boschetti, and J. Legenne, "GNSS time offset—Effects on GPS-Galileo interoperability performance," *Inside GNSS*, vol. 2, no. 6, pp. 60–70, Sep. 2007.
[48] B. Park, "A study on reducing temporal and spatial decorrelation effect in GNSS augmentation system: Consideration of the correction message standardization," Ph.D. dissertation, Dept. Mech. Aerosp. Eng., Seoul Nat. Univ., Seoul, South Korea, Feb. 2008.
[49] W. Ding and J. Wang, "Precise velocity estimation with a stand-alone GPS receiver," *J. Navigat.*, vol. 64, no. 2, pp. 311–325, Apr. 2011.
[50] P. Freda, A. Angrisano, S. Gaglione, and S. Troisi, "Time-differenced carrier phases technique for precise GNSS velocity estimation," *GPS Solutions*, vol. 19, no. 2, pp. 335–341, Apr. 2015.
[51] B. K. H. Soon, S. Scheding, H.-K. Lee, H.-K. Lee, and H. Durrant-Whyte, "An approach to aid INS using time-differenced GPS carrier phase (TDCP) measurements," *GPS Solutions*, vol. 12, no. 4, pp. 261–271, Sep. 2008.
[52] G. W. Roberts, "Noise comparison of triple frequency GNSS carrier phase, Doppler and pseudorange observables," *Measurement*, vol. 144, pp. 328–344, Oct. 2019.
[53] B. Park et al., "RRC unnecessary for DGPS messages," *IEEE Trans. Aerosp. Electron. Syst.*, vol. 42, no. 3, pp. 1149–1160, Jul. 2006.
[54] C. Kee, B. Park, J. Kim, A. Cleveland, M. Parsons, and D. Wolfe, "A guideline to establish DGPS reference station requirements," *J. Navigat.*, vol. 61, no. 1, pp. 99–114, Jan. 2008, doi: 10.1017/S0373463307004304.
[55] *Minimum Aviation System Performance Standards for the Local Area Augmentation System (LAAS)*, document RTCA/DO-245, Radio Technical Commission for Aeronautics (RTCA) Special Committee 159, 2004.
[56] L. Yi-Ting et al., "A fast gradual fault detection method for underwater integrated navigation systems," *J. Navigat.*, vol. 69, no. 1, pp. 93–112, 2016.
[57] Y. Yun, H. Yun, D. Kim, and C. Kee, "A Gaussian sum filter approach for DGNSS integrity monitoring," *J. Navigat.*, vol. 61, no. 4, pp. 687–703, Oct. 2008.
[58] H. J. Seok and B. W. Park, "Prediction of the available time for the SBAS navigation of a drone in urban canyon with various flight heights," *J. Cadastre Land Informatix*, vol. 46, no. 1, pp. 133–148, Jun. 2016.
[59] GNSS Asia. *European GNSS in a Multi-GNSS Environment*. Accessed: Mar. 20, 2023. [Online]. Available: https://gnss.asia/european-gnss/multi-gnss/
[60] H. J. Seok and B. W. Park, "Annual prediction of multi-GNSS navigation performance in urban canyon," *J. Korean Soc. Surveying, Geodesy, Photogramm. Cartogr.*, vol. 34, no. 1, pp. 71–78, Feb. 2016.
[61] G. S. Jeong and S. H. Kong, "GIS based advanced positioning technique for mobile GPS," *J. Korean Inst. Commun. Inf. Sci.*, vol. 40, no. 11, pp. 2261–2290, Nov. 2015.
[62] C. Lim, H. Yoon, A. Cho, C.-S. Yoo, and B. Park, "Dynamic performance evaluation of various GNSS receivers and positioning modes with only one flight test," *Electronics*, vol. 8, no. 12, p. 1518, Dec. 2019, doi: 10.3390/electronics8121518.
[63] H. Yoon, H. Seok, C. Lim, and B. Park, "An online SBAS service to improve drone navigation performance in high-elevation masked areas," *Sensors*, vol. 20, no. 11, p. 3047, May 2020, doi: 10.3390/s20113047.

Yongjun Lee (Graduate Student Member, IEEE) received the B.S. and M.S. degrees from Sejong University, Republic of Korea, where he is currently pursuing the joint Ph.D. degree with the Department of Aerospace Engineering and the Department of Convergence Engineering for Intelligent Drone. His research interests include GNSS, multipath, urban positioning, and machine learning.

Yoola Hwang received the B.S. degree from Yonsei University, Seoul, South Korea, the M.S. degree in aeronautics and astronautics from Purdue University, West Lafayette, and the Ph.D. degree in aerospace engineering sciences from the University of Colorado, Boulder, USA. She joined ETRI in 2004, where she developed the flight dynamics of ground control system of the LEO and GEO satellites and researched GNSS module of UAV. Recently, she is involving in Korean Positioning System (KPS) Development Project.

Jae Young Ahn received the B.S., M.S., and Ph.D. degrees in engineering from Yonsei University, Seoul, South Korea, in 1983, 1985, and 1989, respectively.

He joined ETRI in 1989, where he developed the satellite communications systems, wireless LAN technologies, and radio transmission schemes for mobile communications, from 1989 to 2016. Since 2017, he has been involving in autonomous unmanned vehicle research projects.

Jiwon Seo (Member, IEEE) received the B.S. degree in mechanical engineering from the Korea Advanced Institute of Science and Technology, Daejeon, South Korea, in 2002, the M.S. degree in aeronautics and astronautics in 2004, the M.S. degree in electrical engineering in 2008, and the Ph.D. degree in aeronautics and astronautics from Stanford University, Stanford, CA, USA, in 2010. He is currently an Associate Professor with the School of Integrated Technology, Yonsei University, Incheon, South Korea. His research interests include complementary positioning, navigation, and timing systems, global navigation satellite system (GNSS) anti-jamming technologies, and ionospheric effects on GNSS. He is also a member of the International Advisory Council of the Resilient Navigation and Timing Foundation, Alexandria, VA, USA, and a member of several advisory committees of the Ministry of Oceans and Fisheries and the Ministry of Land, Infrastructure and Transport, Republic of Korea.

Byungwoon Park (Member, IEEE) received the B.S., M.S., and Ph.D. degrees from Seoul National University, Seoul, Republic of Korea. From 2010 to 2012, he worked as a Senior and Principal Researcher with the Spatial Information Research Institute, Korea Cadastral Survey Corporation. Since 2012, he has been an Associate Professor with the School of Aerospace Engineering, Sejong University. His research interests include wide area DGNSS (WAD) correction generation algorithms, geodesy, real-time kinematics (RTK)/network RTK related algorithms, and estimation of ionospheric irregularity drift velocity using ROT variation and spaced GNSS receivers.